NIR-II fluorescence imaging-guided colorectal cancer surgery targeting CEACAM5 by a nanobody

Xiaoyong Guo,[a,b,k] Changjian Li,[c,d,k] Xiaohua Jia,[b,k] Yawei Qu,[e,f,k] Miaomiao Li,[a,b] Caiguang Cao,[b,g] Zeyu zhang,[c,d] Qiaojun Qu,[b,h] Shuangling Luo,[b,i] Jianqiang Tang,[j,****] Haifeng Liu,[a,f,***] Zhenhua Hu,[b,g,**] and Jie Tian[b,c,d,g,*]

[a]Clinical College of Armed Police General Hospital of Anhui Medical University, Department of Gastroenterology of The Third Medical Center of Chinese PLA General Hospital, Beijing, 100039, China
[b]CAS Key Laboratory of Molecular Imaging, Beijing Key Laboratory of Molecular Imaging, Institute of Automation, Chinese Academy of Sciences, Beijing, 100190, China
[c]School of Engineering Medicine, Beihang University, Beijing, 100191, China
[d]Key Laboratory of Big Data-Based Precision Medicine (Beihang University), Ministry of Industry and Information Technology, Beijing, 100191, China
[e]Department of Control Science and Engineering, Harbin Institute of Technology, Harbin, Heilongjiang, 150001, China
[f]Beijing Mentougou District Hospital, Beijing, 102300, China
[g]School of Artificial Intelligence, University of Chinese Academy of Sciences, Beijing, 100049, China
[h]College of Medical Imaging, Shanxi Medical University, Taiyuan, 030001, China
[i]Department of Colorectal Surgery, The Sixth Affiliated Hospital of Sun Yat-Sen University, Guangzhou, 510655, China
[j]Department of Colorectal Surgery, National Cancer Center/National Clinical Research Center for Cancer/Cancer Hospital, Chinese Academy of Medical Sciences and Peking Union Medical College, Beijing 100021, China

eBioMedicine
2023;89: 104476
Published Online xxx
https://doi.org/10.1016/j.ebiom.2023.104476

Summary

Background Surgery is the cornerstone of colorectal cancer (CRC) treatment, yet complete removal of the tumour remains a challenge. The second near-infrared window (NIR-II, 1000–1700 nm) fluorescent molecular imaging is a novel technique, which has broad application prospects in tumour surgical navigation. We aimed to evaluate the ability of CEACAM5-targeted probe for CRC recognition and the value of NIR-II imaging-guided CRC resection.

Methods We constructed the probe 2D5-IRDye800CW by conjugated anti-CEACAM5 nanobody (2D5) with near-infrared fluorescent dye IRDye800CW. The performance and benefits of 2D5-IRDye800CW at NIR-II were confirmed by imaging experiments in mouse vascular and capillary phantom. Then mouse colorectal cancer subcutaneous tumour model (n = 15), orthotopic model (n = 15), and peritoneal metastasis model (n = 10) were constructed to investigate biodistribution of probe and imaging differences between NIR-I and NIR-II *in vivo*, and then tumour resection was guided by NIR-II fluorescence. Fresh human colorectal cancer specimens were incubated with 2D5-IRDye800CW to verify its specific targeting ability.

Findings 2D5-IRDye800CW had an NIR-II fluorescence signal extending to 1600 nm and bound specifically to CEACAM5 with an affinity of 2.29 nM. *In vivo* imaging, 2D5-IRDye800CW accumulated rapidly in tumour (15 min) and could specifically identify orthotopic colorectal cancer and peritoneal metastases. All tumours were resected under NIR-II fluorescence guidance, even smaller than 2 mm tumours were detected, and NIR-II had a higher tumour-to-background ratio than NIR-I (2.55 ± 0.38, 1.94 ± 0.20, respectively). 2D5-IRDye800CW could precisely identify CEACAM5-positive human colorectal cancer tissue.

Interpretation 2D5-IRDye800CW combined with NIR-II fluorescence has translational potential as an aid to improve R0 surgery of colorectal cancer.

Fundings This study was supported by Beijing Natural Science Foundation (JQ19027), the National Key Research and Development Program of China (2017YFA0205200), National Natural Science Foundation of China (NSFC)

*Corresponding author. CAS Key Laboratory of Molecular Imaging, Beijing Key Laboratory of Molecular Imaging, Institute of Automation, Chinese Academy of Sciences, No. 95 Zhongguancun East Road, Hai Dian District, Beijing, 100190, China.
**Corresponding author. CAS Key Laboratory of Molecular Imaging, Beijing Key Laboratory of Molecular Imaging, Institute of Automation, Chinese Academy of Sciences, No. 95 Zhongguancun East Road, Hai Dian District, Beijing, 100190, China.
***Corresponding author. Clinical College of Armed Police General Hospital of Anhui Medical University, Department of Gastroenterology of The Third Medical Center of Chinese PLA General Hospital, No. 69 Yongding Road, Hai Dian District, Beijing, 100039, China.
****Corresponding author. National Cancer Center/National Clinical Research Center for Cancer/Cancer Hospital, Chinese Academy of Medical Sciences and Peking Union Medical College, Beijing, 100021, China.
E-mail addresses: jie.tian@ia.ac.cn (J. Tian), zhenhua.hu@ia.ac.cn (Z. Hu), haifengliu333@163.com (H. Liu), doc_tjq@hotmail.com (J. Tang).
[k]These authors contributed equally to this work.

(61971442, 62027901, 81930053, 92059207, 81227901, 82102236), Beijing Natural Science Foundation (L222054), CAS Youth Interdisciplinary Team (JCTD-2021-08), the Strategic Priority Research Program of the Chinese Academy of Sciences (XDA16021200), the Zhuhai High-level Health Personnel Team Project (Zhuhai HLHPTP201703), the Fundamental Research Funds for the Central Universities (JKF-YG-22-B005) and Capital Clinical Characteristic Application Research (Z181100001718178). The authors would like to acknowledge the instrumental and technical support of the multi-modal biomedical imaging experimental platform, Institute of Automation, Chinese Academy of Sciences.

Keywords: Second near-infrared window; Colorectal cancer; Molecular imaging; CEACAM5; Nanobody

Research in context

Evidence before this study

Complete colorectal cancer resection remains challenging for surgeons. The second near-infrared window (NIR-II, 1000–1700 nm) fluorescence imaging is a novel imaging technique that can visualize tumours at the molecular and cellular level, and assist surgeons to achieve accurate tumour localization and resection. We performed a systematic search of Embase, Medline, and Cochrane databases from their inception date to 27 September 2022 for the terms "fluorescence-guided surgery", "near-infrared fluorescence", and "colorectal cancer". The vast majority of current studies on fluorescence-guided surgery focus on the first near-infrared window (NIR-I, 700–900 nm). NIR-II window has advantage with deeper penetration depth and higher resolution and lower background than NIR-I, however, there is a lack of studies on the use of NIR-II fluorescence imaging for intraoperative navigation of colorectal cancer.

Added value of this study

In this study, we established 2D5-IRDye800CW, an NIR-II targeting probe, which can specifically recognize CEACAM5-positive colorectal cancer. We constructed a variety of colorectal cancer animal models and used human samples to verify the targeting of the probe and the value of NIR-II imaging for colorectal cancer intraoperative navigation.

Implications of all the available evidence

Our study provides a new technical means for NIR-II fluorescence imaging to be used in colorectal cancer surgery. It helps to discover and identify deeper vessels and small peritoneal metastases, which can assist surgeons in accurate tumour resection. In addition, our probe is composed of nanobody with high affinity and low immunogenicity conjugated to conventional near-infrared fluorescent dye IRDye800CW, which shows great potential for clinical translation.

Introduction

Colorectal cancer (CRC) is one of the cancers with the highest morbidity and mortality worldwide.[1,2] Radical surgical resection of all tumour tissue with clear margins remains the mainstay of treatment in the majority of colorectal cancer patients, and complete surgical tumour resection (R0) is associated with better overall survival and lower recurrence rates.[3] However, R0 resection remains challenging in many patients. Tumour-positive resection margins have been reported in 5% of colon cancer cases, but the incidence is higher with increasing tumour stage, up to 14% in T4 colon cancer. In addition, in locally advanced rectal cancer, the proportion of positive tumour margins was 28%, 35% rectal cancer occurred incomplete tumour resection. This rate was even higher in patients with recurrent rectal cancer, with positive resection margins reported in up to 50% of tumours.[3–6] Moreover, approximately 3–20% of colorectal cancer patients develop peritoneal metastases (PM),[7] and international standards recommend cytoreductive surgery combined with intraperitoneal hyperthermia chemotherapy (CRS-HIPEC) as a potentially curative procedure. The completeness of cytoreduction is directly associated with survival[8]; therefore, maximal cytoreduction of small and otherwise undetected tumour lesions is important. In these cases, it is difficult to accurately distinguish adhesions or fibrosis and tumour lesions because the surgeon can only rely on visual and tactile information, and there is a lack of real-time intraoperative imaging technology to assist the surgeon in distinguishing between malignant and benign tissue.[9,10]

Near-infrared (NIR) fluorescence imaging is a real-time imaging technology that combines near-infrared fluorescent targeted probes with a fluorescence imaging system to distinguish tumour from normal tissue by identifying specific and highly expressed molecular targets on tumour tissue.[11–13] Several clinical studies of NIR-targeted probes have been reported for malignancies (colorectal, pancreatic, and ovarian),[14–16] metastases (liver and peritoneum),[17,18] and vital anatomical structures (nerves, etc.).[19] Conventional fluorescence-guided surgery focuses on the first near-infrared window (NIR-I, 700–900 nm), which has limited tissue penetration depth

of only 1–6 mm.[20–22] However, the second near-infrared window (NIR-II, 1000–1700 nm) significantly overcomes the effects of strong tissue absorption, autofluorescence, and photon scattering to afford deep tissue penetration (up to 20 mm), micron-scale spatial resolution, and high tumour-to-normal tissue (T/NT, more than 190),[23–29] which is promising to improve T/NT and tumour margin determination, allowing more precise tumour resection. CEACAM5 is overexpressed in 90% of CRC, and the expression of CEACAM5 in normal tissue is on average 60-fold lower than in tumour tissue, making it an optimal imaging target for CRC.[30,31]

Although many NIR-II fluorescent probes with excellent imaging performance have been reported, the clinical conversion potential of existing NIR-II targeted probes is still limited due to the unknown immunogenicity of current fluorescent dyes.[32,33] To the best of our knowledge, the application of NIR-II to CRC intraoperative navigation has not been reported yet. Therefore, in this study, we conjugated the anti-CEACAM5 nanobody (2D5)[34] with the near-infrared fluorescent dye IRDye800CW to construct a targeted NIR-II probe: 2D5-IRDye800CW to explore the value of NIR-II fluorescence in intraoperative navigation of colorectal cancer.

Methods

Ethics statement

This study was approved by the medical ethics review team of the third medical center of Chinese PLA General Hospital (ethics number: 2022-27). Informed consent was obtained from all participants included in the study. All animal experiments were performed in line with the principles of the Declaration of Helsinki.

2D5-IRDye800CW synthesis and characterization

A 5-fold molar excess of IRDye800CW NHS (LI-COR Bioscience) (dissolved at 10 mg/ml in DMSO) was incubated with anti-CEACAM5 nanobody (2D5, Shenzhen Guochuang Nanobody Technology Co., Ltd.) (1 mg/ml) for 2 h at pH 8.5 in the dark. Unbound IRDye800CW NHS was eluted by size exclusion chromatography using a Superdex 75 10/300 GL column (GE Healthcare) with PBS (pH 7.4) as an elution buffer (0.5 ml/min). The concentration and fluorescence binding ratio of labeled nanobody and the absorption spectra was determined on a Shimadzu UV-2600 UV-Vis spectrophotometer, and the emission spectra were measured on FLS980 (Edinburgh Instruments). Affinity was determined using surface plasmon resonance (Biacore T200, GE Healthcare) on 2D5-IRDye800CW proteins immobilized on a CM5 chip (GE Healthcare).

NIR-I/II imaging of blood vessels and capillary phantom

All animals purchased from Beijing Vital River Laboratory Animal Technology Co., Ltd. The head and right hindlimb of 8-week-old C57BL6 male mice were used for depilation, and 2D5-IRDye800CW (1–5 mg/kg) was administrated via tail vein; then, the NIR-II camera (Xenics Cheetah-640CL TE3) was used for imaging. The filters were selected at 1000 nm, 1100 nm, 1200 nm, 1300 nm and 1400 nm, and the excitation laser was 808 nm with the exposure time of 30 ms∼1 s. NIR-I imaging was performed with CMOS, PCO camera, and a bandpass filter of 850 ± 40 nm was connected to capture NIR-I fluorescence. The excitation wavelength was 792 nm and the exposure time was 30 ms. After the images were acquired, the contrast within the region of interest containing blood vessels in NIR-I and NIR-II imaging was quantified by calculating the cross-section fluorescence intensity. For the phantom experiment, 0.01 mg/ml 2D5-IRDye800CW was injected into a capillary glass tube with an inner diameter of 1 mm, soaked with 2% fat emulsion, and the depth was 5 mm for NIR-I/II imaging. All signal intensity profile was Gaussian fitted in the Origin software (OriginPro 2018C, OriginLab).

Western blot and immunofluorescence

The human CRC cell lines HT29-*Luc* (BNCC, Cat# BNCC353700, RRID: CVCL_5J20), colo201 (BNCC, Cat# BNCC360304, RRID: CVCL_F399) and SW480 (BNCC, Cat# BNCC100604, RRID: CVCL_0546) were purchased from BeNa Culture Collection, Henan, China, and colo320 (EK-Bioscience, Cat# CC-Y1568, RRID: CVCL_1989) was purchased from Shanghai EK-Bioscience Biotechnology Co., Ltd. The Cells were lysed in RIPA buffer with protease and protein phosphatase inhibitors, and protein concentrations were determined using the BCA protein (G5001, Servicebio, Wuhan, China) assay kit. Protein samples were then boiled for 10 min, and 20 μg of total protein was electrophoresed on a 10% SDS-polyacrylamide gel and transferred onto PVDF membranes. Blocking of the membrane with a 5% BSA was done for 2 h at room temperature (RT). Immunoblotting was performed overnight using a 1:500 dilution of anti-CEACAM5 antibody (Abcam Cat# ab133633, RRID: AB_2924882) in a refrigerator at 4 °C, and GAPDH (GB12002, Servicebio, Wuhan, China) was used as an endogenous control. The samples were washed in TBST for three times, and incubated with a secondary antibody conjugated with goat polyclonal secondary antibody to rabbit IgG-HRP (GB23303; Service-bio, Wuhan, China) for about 1 h at RT. Finally, CEACAM5 expression was detected by using enhanced chemiluminescence, imaged by an Alliance MINI HD 6 analyzer (UVITEC, UK) and calculated by quantifying western blot band intensities using the ImageJ Gel Analyzer plugin. We used PKH26 cell membrane staining (Sigma Aldrich, MINI26) and immunofluorescence to locate the subcellular location of CEACAM5 and the probe. The cells in the exponential

growth phase were digested and the cell membrane was stained according to the instructions for PKH26. Then, the cell concentration was adjusted to $1\sim5 \times 10^5$/ml with a complete medium; and cells were evenly spread on 15mm confocal dishes containing a 0.5ml medium. After cell adhesion, incubated with 0.01 mg/ml 2D5-IRDye800CW for 2 h at RT, then wished with PBS three times, fixed with 4% Paraformaldehyde Fix Solution (PFA) for 10 min, washed twice with PBS, 5% BSA was added, and cells were blocked at RT for 30 min. Adding the diluted (1:2000) Alexa Fluor®488 Anti-CEACAM5 antibody (Abcam Cat# ab214868, RRID: AB_2924884) and refrigerating was done at 4 °C overnight. Washing with PBS in the dark for 3 × 5 min, adding DAPI counterstaining for 5 min, and imaging with laser confocal microscope was done.

In vitro targeting evaluation

Three CRC cell lines HT29-*Luc*, SW480, colo201 and normal colon epithelial cell line NCM460 (EK-Bioscience, Cat# CC-Y1550, RRID: CVCL_0460) were cultured. SW480 was cultured in L15 + 10% FBS + 1% penicillin/streptomycin (P/S) at 37 °C in 100% air. HT29-*Luc*, colo201 and NCM460 were cultured in RPMI 1640 medium and DMEM containing 10% FBS and 1% P/S at 37 °C in 5% CO_2. Approximately 5×10^5/ml cells were evenly spread in a 15 mm glass bottom petri dish containing 1 ml of culture medium. After the cells grew to the required density (70%–90%), 2D5-IRDye800CW 200 μL of 0.01 mg/ml was added, and cells were incubated for 2 h at RT in the dark, washed with PBS 3 times, fixed with 4% PFA for 10 min, and stained with DAPI for 10 min. Observations were made with a laser confocal microscope (LSM780, Carl Zeiss, Jena, Germany). For the binding site competition blocking experiment, cells were incubated with 2D5 unlabeled with IRDye800CW at 100 times probe concentration for 2 h, washed three times with PBS, and then incubated with 200 μL of 2D5-Irdye800CW at 0.01 mg/ml. Nucleus was stained with DAPI and observed by laser confocal microscopy.

Immunohistochemical staining and HE staining

Fresh tissue was placed in a cryotome cryostat for section. Fixed the tissue sections with cold acetone at 4 °C. Socked the slides in 3% H_2O_2 solution in PBS at RT for 10 min to block endogenous peroxidase activity. Incubated the samples in 5% BSA blocking solution at 37 °C for 30 min. Then add properly diluted primary antibody to cover the samples (1:400 dilution, Abcam Cat# ab4539, RRID: AB_304505). Incubated overnight at 4 °C in a wet box. Cover the samples with properly diluted secondary antibody (1:1000, ThermoFisher, Cat# A10551) at RT after PBS washing. Place sections in solution for DAB reaction. The clinical tumour tissue samples were obtained from clinical surgery, and stored in 4% paraformaldehyde after *in vitro* imaging. The tissue sections were embedded with embedding agent, frozen, fixed after sectioning, and stained with hematoxylin and eosin (H&E) for pathological analysis.

Nude mouse colorectal cancer xenograft models

All the mice were purchased from Beijing Vital River Laboratory Animal Technology Co., Ltd. Approximately 5×10^6 colorectal cancer cells were mixed with 125 μL PBS and then inoculated into the right lower back of BALB/c nude mice to construct a subcutaneous tumour model. Imaging was performed when the tumour grew to 0.5 cm–1.0 cm. For the orthotopic model of colorectal cancer, the nude mice were anesthetized and the cecum was exposed by surgical procedures. A 25G standard 1 ml insulin syringe was used to draw 50 μL of cell suspension (1×10^5), then the needle was slowly inserted between the cecal serosa and the muscularis layer to inject cells, and finally the peritoneum and skin were sutured in layers. The entire process was completed on a sterile ultra-clean bench.

Bioluminescence imaging

Bioluminescence imaging (BLI) was performed using the IVIS Spectrum In Vivo Imaging System (Caliper Life Sciences, Waltham, Massachusetts) to locate the tumour. Tumour-bearing mice were anesthetized with 2% isoflurane and then received an intraperitoneal injection with 150 mg/kg D-luciferin in 100 μL of normal saline; BLI images were acquired 10 min after D-luciferin injection.

NIR-I/II fluorescence imaging

2D5-IRDye800CW at a dose of 3 μg/g was administered through the tail vein into tumour bearing mice. NIR-I fluorescence imaging was performed with a Complementary Metal Oxide Semiconductor (CMOS) camera (PCO. edge 5.5, PCO, Germany) and IVIS Spectrum In Vivo Imaging System. To obtain NIR-I fluorescence, a long-pass filter with the cutoff wavelength of 850 nm (FEL0850, Thorlabs, USA) was connected with the lens. The wavelength of the excitation laser was 792 nm with the power set to be 20 mW/cm^2, and the exposure time was 30 ms. NIR-II fluorescence imaging was implemented with an InGaAs SWIR camera (Xenics Cheetah-640CL TE3) coordinated with a lens (Spacecom VF50M SWIR) that can transmit NIR-II light, and a filter wheel (1000 nm, 1100 nm, 1200 nm, 1300 nm, 1400 nm, 1500 nm, Thorlabs, USA) was fixed in the front end of the lens to capture NIR-II fluorescence. The wavelength of the excitation laser was 808 nm with the power set to be 50 mW/cm^2, and the exposure time was 0.5–2 s. The blocking group was injected with unlabeled 2D5 at a dose of 100 μg/g, and 10min later, 2D5-IRDye800cw was administrated with body weight of 3μg/g for fluorescence imaging. The fluorescence intensity was measured by the software ImageJ, and tumour-background ratio

(TBR) is defined as the ratio of fluorescence intensity between tumour and peritumoral tissue.

Ex vivo molecular imaging of fresh human CRC specimen

We collected endoscopic biopsy CRC specimens (n = 5), and intraoperatively resected CRC tumour with adjacent normal tissue (n = 10) at the Third Medical Center of Chinese PLA General Hospital, patient and tumor characteristics are in the supplementary materials (Table S1). We did not specifically analyze the effects of different genders on the experiment, but it is necessary to analyze different genders.[35] The fresh specimens were preserved in a tissue preservation solution, and then the blood stains on the specimen's surface were washed with PBS. CRC specimens were incubated with 2D5-IRDye800CW at a concentration of 10 μg/ml for 30 min, and normal tissue specimens were used as control. After incubation, tissue specimens were rinsed three times with PBS and imaged with an NIR-II camera. Specimens were further frozen and sectioned to a thickness of 6 μm, and the sections were blocked with 5% fetal bovine serum for 30 min under RT, then incubated with 2D5-IRDye800CW (10 μg/ml) for 20 min at RT, washed three times with PBS, and sealed with anti-fluorescence quenching tablet (including DAPI). Finally, three consecutive sections were cut for HE and CEACAM5 immunohistochemical staining.

Statistical analysis

The NIR fluorescence images were quantitatively analyzed using ImageJ software (National Institutes of Health) and converted into pseudo color. The experimental data was expressed as mean ± standard deviation (SD), and the comparison between the two groups was evaluated by *Student's t test* (GraphPad Prism 7, *P < 0.05 considered significant, *, **, ***, and **** represents P < 0.05, P < 0.01, P < 0.001, and P < 0.0001, respectively) because of the two groups of data come from normally distributed populations, and the variance of the data is homogeneous, which satisfies the independence. The apparent width of the corresponding capillary was calculated using the Gaussian fitting full width Half maximum (FWHM) by the Origin software (OriginPro 2018C, OriginLab).[23] Immunohistochemical staining was scored by three pathologists alone, H-Score = $\sum$(pi × i) = (percentage of weak intensity × 1) + (percentage of moderate intensity × 2) + (percentage of strong intensity × 3), where pi represents the ratio of positive signal pixel area to cell number; i stands for tint intensity.

Role of the funding source

The sponsors of the study had no role in the study design, data collection, data analyses, data interpretation, manuscript writing, or the decision to submit the paper for publication.

Results

Characterization of 2D5-IRDye800CW

The imaging probe 2D5-IRDye800CW was obtained by conjugated IRDye800CW with the anti-CEACAM5 nanobody (2D5) through random site labeling (Fig. 1a). The optical density (OD) value of 774 nm and 280 nm at different concentrations was measured and standard curves were drawn (Fig. 1b). According to the formula previously reported,[36] the ratio of fluorescence to protein was 1.25, that is, 1.25 fluorescent dyes were attached to an average nanobody. The affinity of 2D5-IRDye800CW was determined by surface plasmon resonance, Kd = 2.29 nM (Fig. 1c). The absorption spectrum and the NIR-I emission spectrum of 2D5-IRDye800CW were further determined, among which the peak value of the absorption spectrum was 776 nm and the peak value of emission was 789 nm. According to a previous report,[37] IRDye800CW had NIR-II emission trailing, so the emission spectrum of 2D5-IRDye800CW in NIR-II was determined, and 2D5-IRDye800CW still had the NIR-II signal at 1600 nm (Fig. 1d and e). In addition, the relationship between the concentration of 2D5-IRDye800CW and the fluorescence intensity was determined. Within a certain range of concentration, the NIR-I or NIR-II fluorescence intensity of 2D5-IRDye800CW was linearly related to the concentration, y = 1610*x+3318, R^2 = 0.99, y = 3330* x+6298, R^2 = 0.95, respectively (Fig. 1f and g).

NIR-II imaging of 2D5-IRDye800CW in blood vessels and capillary phantom

To verify the NIR-II imaging advantage of 2D5-IRDye800CW, the vascular imaging of the mouse head was performed non-invasively through the intact scalp and skull of the mouse. Imaging of NIR-I at 850 nm revealed only vaguely shaped large vessels after intravenous administration of 2D5-IRDye800CW. While NIR-II imaging at long wavelengths (1000–1300 nm) allowed three clearer blood vessels to be observed (Fig. 2a). Quantitative analysis of fluorescence cross-section intensity distribution showed that, as the wavelength increased from 850 nm to 1300 nm, the peak of NIR-II was higher than that of NIR-I (red dotted line in Fig. 2b). NIR-I/II fluorescence imaging of the hindlimb blood vessels in mice also showed similar results (Fig. 2c). S/N is defined as the ratio of the fluorescence signal value (counts) of blood vessels to the surrounding tissue, and the S/N of the hindlimb vascular imaging of mice was (white arrows): 1.1 at 850 nm; 1.20, 1.25, 1.15 at 1100 nm; 1.35, 1.5, 1.41 at 1300 nm, and 1.3, 1.81, 1.5 at 1400 nm (Fig. 2d). As the wavelength was extended from NIR-I at 850 nm to NIR-II at 1400 nm, the imaging resolution and signal-to-background ratio of tiny blood vessels were improved.

To further verify the benefits of 2D5-IRDye800CW NIR-II imaging in depth and compare the scattering

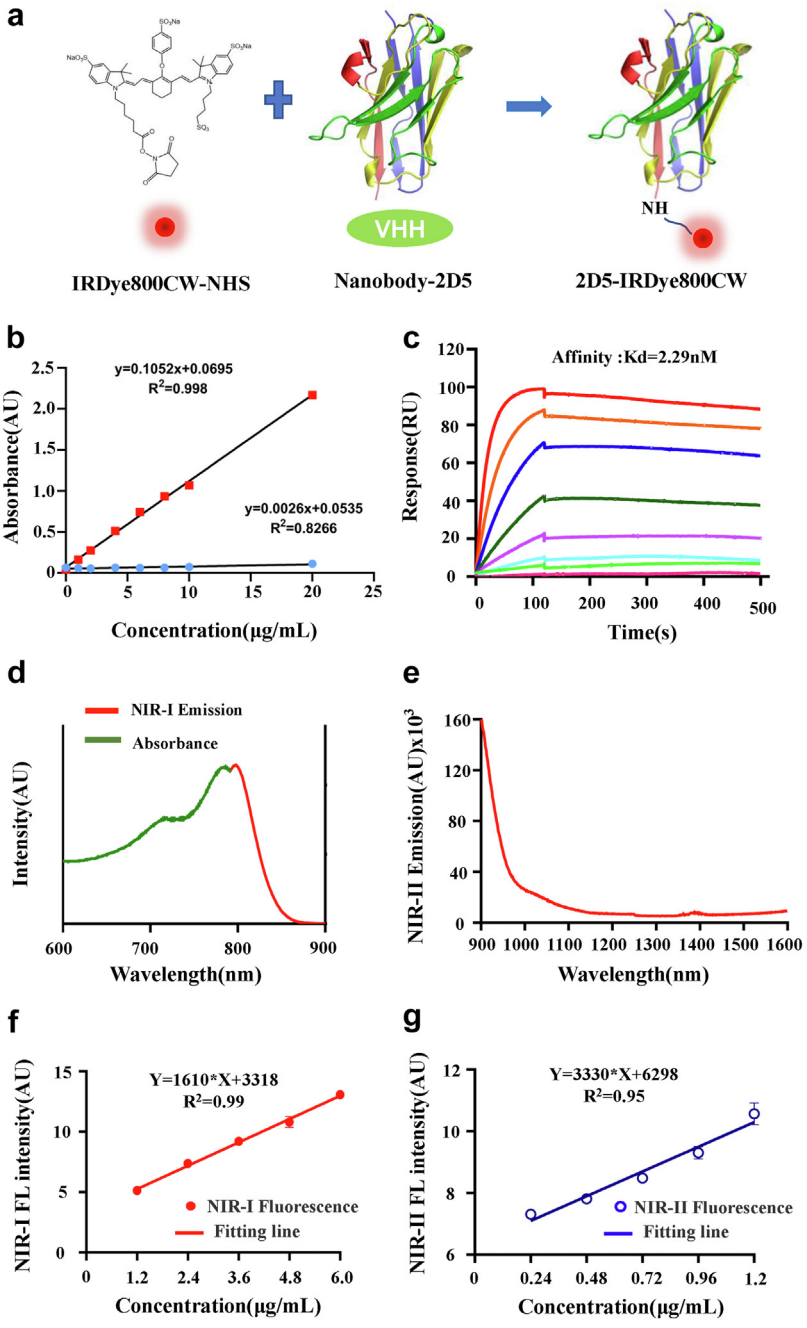

Fig. 1: Characterization of 2D5-IRDye800CW. (a) Conjugation of the nanobody and IRDye800CW dye. (b) Standard curve of UV absorption optical density value at 774 nm and 280 nm. (c) The affinity of probe at different concentration was determined by SPR, Kd = 2.29 nM. (d) Absorption and emission spectra of 2D5-IRDye800CW. (e) Emission spectra in NIR-II spectra after signal intensity normalization. (f, g) The NIR-I/II fluorescence intensity of 2D5-IRDye800CW is linearly related to the concentration within a certain range.

property of photons in different spectra, we filled capillary tube with 2d5-IRDye800CW and immersed in the intralipid solution simulate intestinal tissue and blood vessels. At a depth of 5 mm within the fat, fluorescence was captured in all NIR spectra from 850 nm to 1300 nm, but the most severe scattering was observed in NIR-I imaging (850 nm), whereas NIR-II imaging (1300 nm) was almost non-scattering (Fig. 2e). It is further proved by Gaussian fitting that the same capillary has a lower full width at half maxima (FWHM) at a

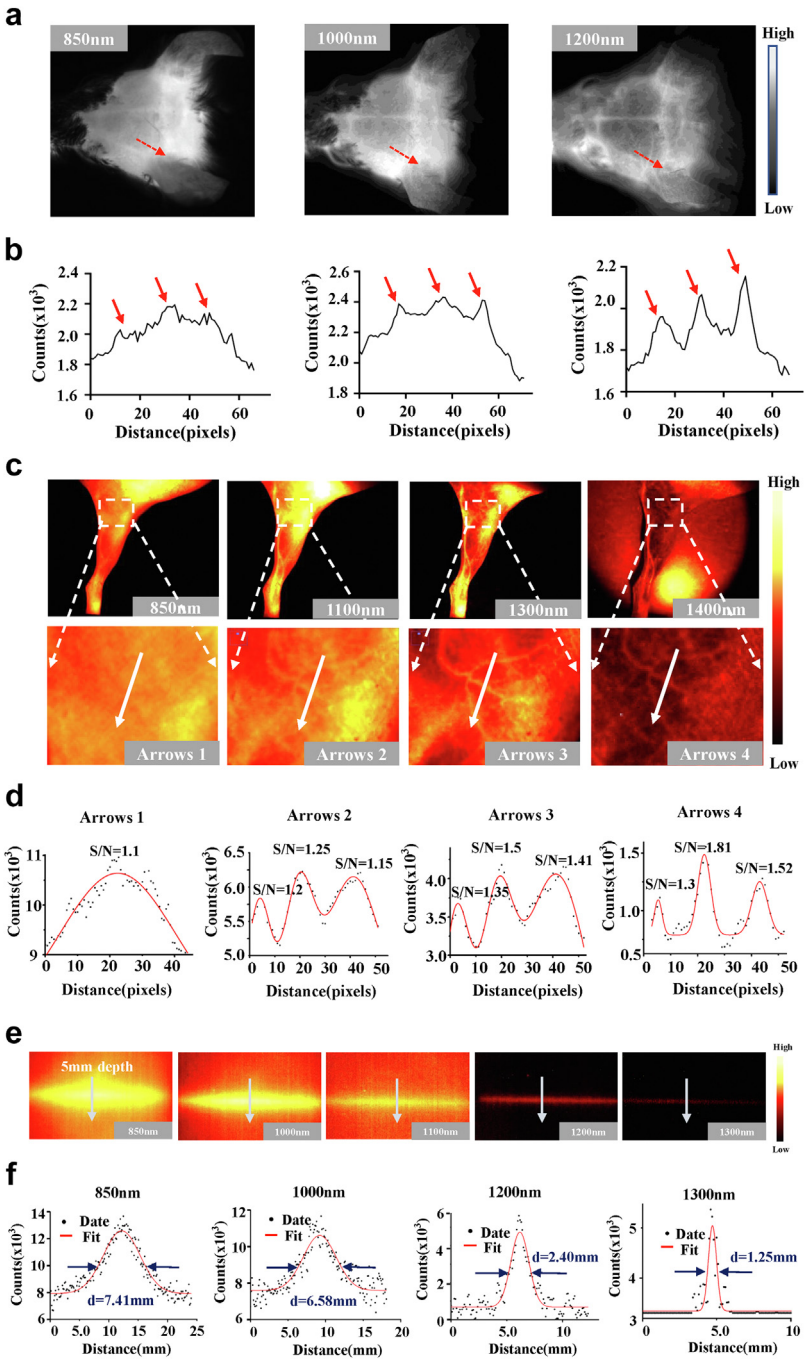

Fig. 2: 2D5-IRDye800CW NIR-II imaging of blood vessels and capillary phantom. (a) The brain vessels of mouse at NIR-I 850 nm bandpass filter and NIR-II 1000 nm and 1200 nm long pass filters. (b) Fluorescence cross-sectional intensity distribution of cerebral vessels in the NIR-I/II window (red dotted line in (a)), and the peak pointed by the red arrow in the curve is the location of the blood vessel (c) NIR-II image of mouse hindlimb vessels with different NIR-II long-pass filters on InGaAs camera. Switching to 1400 nm long-pass NIR-II fluorescence greatly improved vessel contrast. (d) Fluorescence cross-sectional intensity distribution of hindlimbs in NIR-I and NIR-II windows (white arrows in (c)). Gaussian fit to normalized fluorescence intensity with highest S/N at 1400 nm. (e) Comparison of multispectral fluorescence imaging of the same capillary (inner diameter of 1 mm), where the most serious scattering occurred in the spectral band of NIR-I 850 nm at a depth of 5 mm. (f) Gaussian fit of the longitudinal profile of signal intensity (white arrows in (e)). FWHM of the same capillary in each spectrum is 7.41 mm, 6.58 mm, 2.40 mm, and 1.25 mm, respectively.

longer wavelength. At 850 nm, 1000 nm, 1200 nm, and 1300 nm wavelengths, FWHM is 7.41 mm, 6.58 mm, 2.40 mm, and 1.25 mm, respectively, and with the increase of emission wavelength, FWHM was closer to the 1 mm inner diameter of the capillary tube, indicating that this imaging wavelength has less photon scattering (Fig. 2f).

Expression of CEACAM5 in human colorectal cancer cell lines

We measured the expression of CEACAM5 in four human colorectal cancer cell lines HT29-*Luc*, SW480, colo320, and colo201 by western blot. The results showed that HT29-*Luc* and SW480 overexpressed CEACAM5, while colo201 and colo320 did not express CEACAM5 (Fig. 3a). Quantitative analysis showed that the gray value ratio of CEACAM5 bands and internal reference tubulin bands in HT29-*Luc*, SW480, colo320, and colo201 was 2.20, 1.51, 0.01, and 0.01, respectively (Fig. 3b). The cell membrane of SW480 was stained by PKH26 (red) and colocated with the immunofluorescence results of CEACAM5 (green). The results showed that the two stains could colocalization, and the Pearson's correlation coefficient (PCC) value was 0.90. Colocalization of the probe uptake results (yellow) and PKH26 (red) was then performed, which showed a PCC value of 0.85. These results demonstrate that CEACAM5 is distributed on the surface of the cell membrane and that our probe binds to the cell surface (Fig. 3c).

In vitro cellular uptake

We incubated HT29-*Luc*, SW480, NCM460 and colo201 with 2D5-IRDye800CW, respectively. The results showed that HT29-*Luc* and SW480 were bound to the probe (Fig. 3d, red fluorescence), while NCM460 and colo201 were not. Statistical analysis showed that the intensity of probe fluorescence signal of HT29-*Luc* was significantly different from that of other cells ($P < 0.01$, Student's t-test). Binding site blocking experiments further verified the targeting of 2D5-IRDye800CW binding to overexpressing CEACAM5 cells. HT29-*Luc* was blocked by the unlabeled fluorescent nanobody 2D5, and no fluorescent signal was acquired after incubation with 2D5-IRDye800CW, quantitative analysis showed that the fluorescence intensity of the blocking group was significantly lower than that of the HT29-*Luc* group (Fig. 3d).

In vivo specificity and biodistribution of probes

CRC cell lines HT29-*Luc* with CEACAM5 overexpression and colo201 without CEACAM5 expression were used to construct the mouse subcutaneous tumour models, respectively. 2D5-IRDye800CW (2 μg/g mouse body weight) was injected into the tail vein of tumour-bearing mice, and fluorescence images were taken with the NIR-II imaging system to evaluate the specificity and body distribution of the probe. After injection of 2D5-IRDye800CW into subcutaneous tumours constructed with HT29-*Luc* (n = 5), the kidneys showed a strong fluorescent signal that gradually decreased with time. The fluorescent signal was detected in the tumour area after 0.5 hour, and TBR gradually increased with time. The fluorescence signal of the tumour could be clearly seen at 2 hours, and the highest TBR = 2.67 ± 0.24 was reached at 24 hours. The control group colo201 tumour-bearing mice (n = 5) showed no obvious fluorescence signal in the tumour area with TBR = 1.16 ± 0.13 ($P < 0.001$, Student's t-test) (Fig. 4a and b). Another group of mice (n=3) were euthanized at the optimal imaging time point (24 hours), organs and tumours were dissected for *ex vivo* NIR-II imaging, and it was found that 2D5-IRDye800CW was mainly distributed in kidneys, liver and tumour tissue (Fig. 4c).

For imaging of the orthotopic colorectal cancer model constructed by HT29-*Luc* (n = 5), the tumour in the abdominal cavity (indicated by the asterisk) was located by bioluminescence and CT (small animal multimodality imager), and the 3D reconstruction of BLI-CT was performed (Fig. 4d). Then, 2D5-IRDye800CW was administered through the caudal vein, and a surgical procedure was performed to expose the intestine after 24 hours. NIR-I/II imaging showed high fluorescence signal of tumour, and the TBR was 1.6 and 2.1, respectively, as shown by black arrows (Fig. 4e–g). BLI and HE staining were performed after excision of the intestine and the area with high fluorescence signal, which confirmed that the area was tumour tissue with a diameter of 2 and 3 mm (Fig. 4h and i).

NIR-II fluorescence-guided R0 resection of colorectal cancer

The orthotopic mouse model of colorectal cancer was established by HT29-*Luc* (n = 10). 24 hours after administration of 2D5-IRDye800CW, tumours were resected under white light and NIR-II fluorescence guidance, respectively. The abdominal cavity of mice was cut open by tissue shear, and the intestinal tract and peritoneum were fully exposed. It was difficult to distinguish normal tissue from tumour tissue under white light. NIR-II fluorescence imaging showed stronger fluorescence signal in the cecum and peritoneum than normal tissue. Subsequently, the NIR-I imaging signal and BLI signal were collected on the small animal living imager. NIR-I/II imaging and BLI signal were co-localized, indicating that the nodules with a high fluorescence signal were tumour tissue (Fig. 5a–e). Then, the primary lesion was excised under the guidance of NIR-II fluorescence, and a high fluorescence signal area appeared on the peritoneum was also excised (Fig. 5f). NIR-II imaging was performed after excision, and no areas of the high fluorescence signal were found (Fig. 5g). BLI imaging was performed on the post-operative mice, no high signal area appeared in the abdominal cavity of the mice, which proved that there

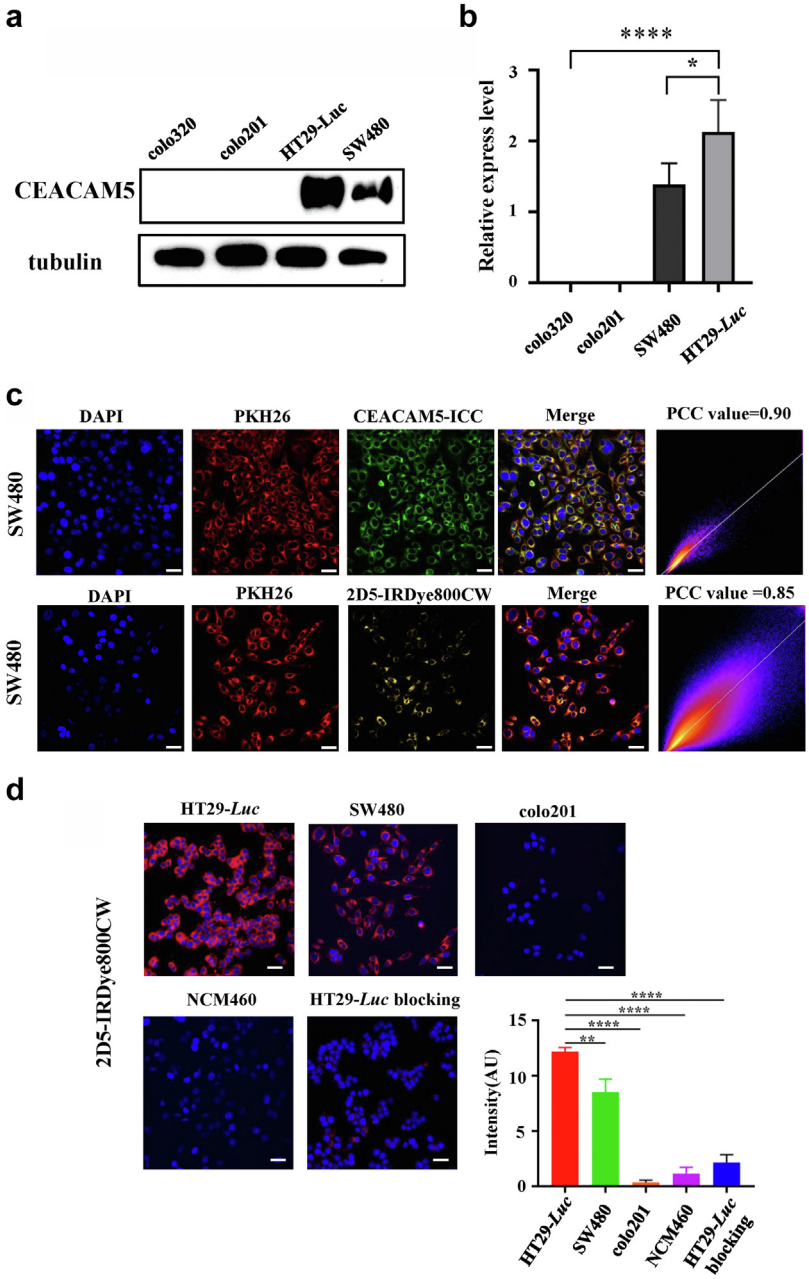

Fig. 3: *In vitro* targeting evaluation. (a, b) HT29-*Luc* and SW480 overexpressed CEACAM5, while colo201 and colo320 did not express CEACAM5. The relative expression level was statistically different (Student's t-test). (c) Cell membrane staining (PKH26, red) and immunocytochemistry (ICC, green) colocalization. Pearson's correlation coefficient (PCC) value = 0.90 (calculated by the analyze-colocalization-coloc 2 plugin in the software ImageJ). PKH26 cell membrane staining and probe incubation results (yellow) colocalization, PCC value = 0.85. Scale bar, 20 μm. (d) 2D5-IRDye800CW uptake by different cell lines (red) and blocking experiment. Nucleus were stained with DAPI (blue). Quantitative analysis of probe fluorescence intensity showed significant difference compared with HT29-*Luc* (t-test). Scale bar, 20 μm.

was no residual tumour tissue, and R0 resection was achieved (Fig. 5h). Quantitative analysis of the two tumour areas identified showed that the larger tumour had higher TBR than the smaller tumour (2.1 *vs.* 1.7, Fig. 5i). Finally, we analyzed the difference between NIR-II and NIR-I imaging tumours in 30 mice, and the results showed that NIR-II had higher TBR (2.55 ± 0.38 *vs.* 1.94 ± 0.20, $P < 0.0001$, Student's t-test, Fig. 5j).

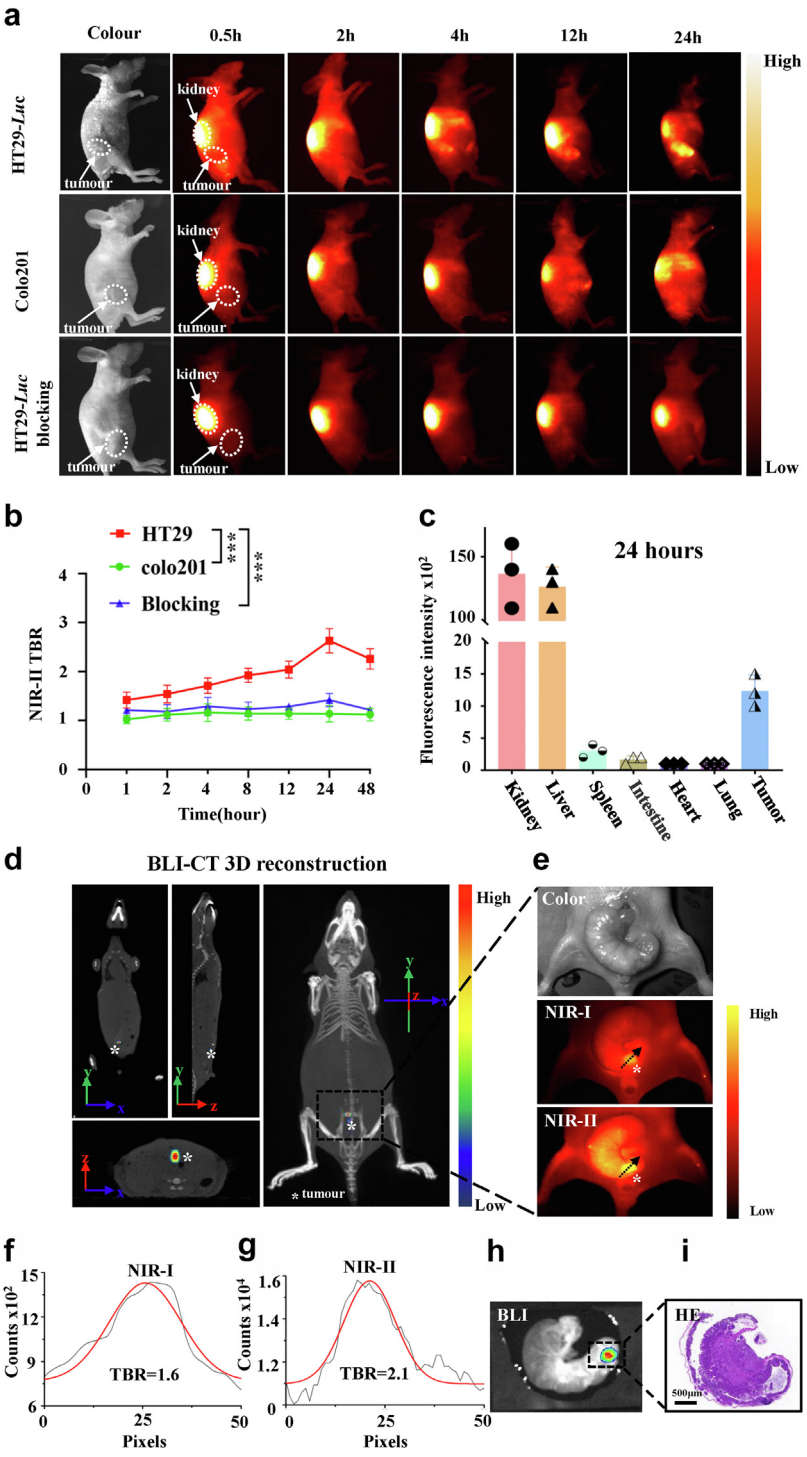

Fig. 4: In vivo specificity and biodistribution of 2D5-IRDye800CW. (a) Representative examples of whole-body imaging at different time points of intravenous injection 2D5-IRDye800CW in HT29-*Luc* and colo201 subcutaneous xenograft tumour models (n = 10) and in HT29-*Luc* subcutaneous tumour blocking experiments (n = 5). (b) Tumour-to-background ratio of NIR-II fluorescence signal intensity, and the skin fluorescence signal intensity around the tumour was selected as the background. Statistical analysis (Student's t-test) with $P < 0.05$ was regarded as statistically significant. (c) 2D5-IRDye800CW distribution in organs after intravenous injection 24 hours. (d) BLI-CT 3D reconstruction of the tumour (white asterisk). (e) NIR-I/II imaging of the orthotopic xenograft tumour (n = 5, orange pseudo-colored fluorescent signal). (f, g) TBR of the tumour NIR-I and NIR-II image, respectively. (h, i) BLI and pathological HE staining after orthotopic tumour resection.

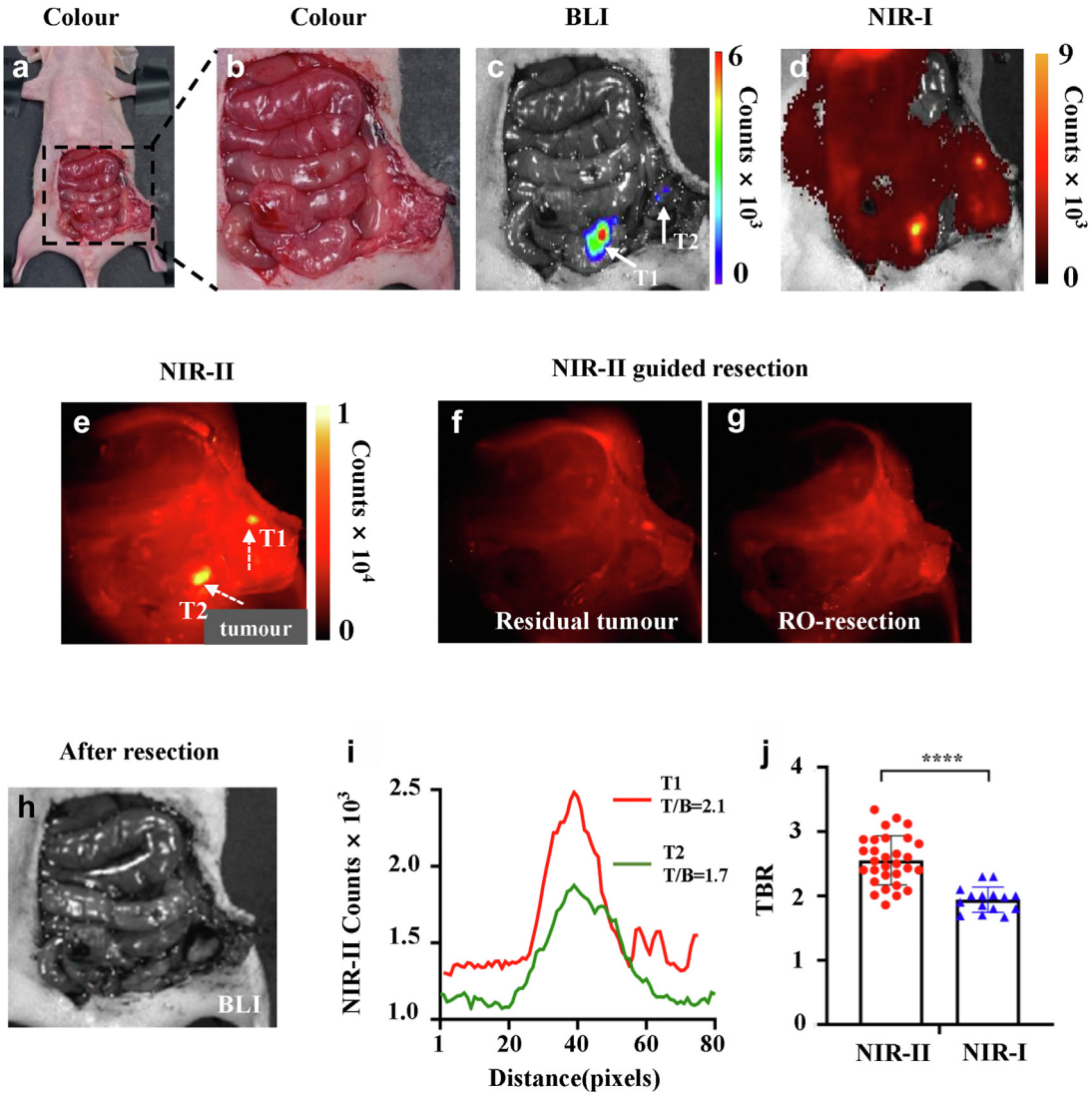

Fig. 5: Representative sample of NIR-II fluorescence-guided R0 resection of colorectal cancer (n = 10). (a–e) Colour image, BLI and NIRI/II fluorescence images were collected after abdominal cavity exposure. (f) NIR-II fluorescence-guided resection of orthotopic colorectal tumour. (g, h) NIR-II and BLI imaging after resection of metastases without tumour remnants. (i) Quantitative analysis of the tumour indicated by the arrow in the (e) to calculate TBR. (j) TBR of tumours in 30 mice, and the results showed that NIR-II had higher TBR (2.55 ± 0.38 *vs.* 1.94 ± 0.20, Student's t test, P < 0.0001).

NIR-II fluorescence-guided surgery for colorectal peritoneal cancer

Optimal cytoreductive surgery combined with hyperthermic intraperitoneal chemotherapy is crucial for the curative treatment of colorectal-derived peritoneal cancer.[38] Therefore, we constructed a colorectal cancer peritoneal metastasis model to evaluate the ability of the probe to identify metastatic lesions (n = 10). 24 hours after probe administration, the abdominal cavity and peritoneum of tumour-bearing mice were fully exposed surgically, and NIR-II imaging showed high fluorescence signal in the cecum and peritoneum, which was higher than normal intestinal tissue. The results of BLI imaging corresponded to NIR-II (Fig. 6a–c). In the first step, the primary colorectal cancer lesion was excised, and residual tumour lesion and peritoneal metastases were visible under NIR-II fluorescence (Fig. 6d). In the second part, after assessing the extent of peritoneal metastases, the residual tumour and peritoneal metastases were all resected (Fig. 6e). BLI imaging was performed after all areas with a high fluorescence signal were resected, which proved that there was no residual tumour tissue (Fig. 6f). Postoperative pathology confirmed that all the resected tissue was tumour tissue, and immunohistochemistry was

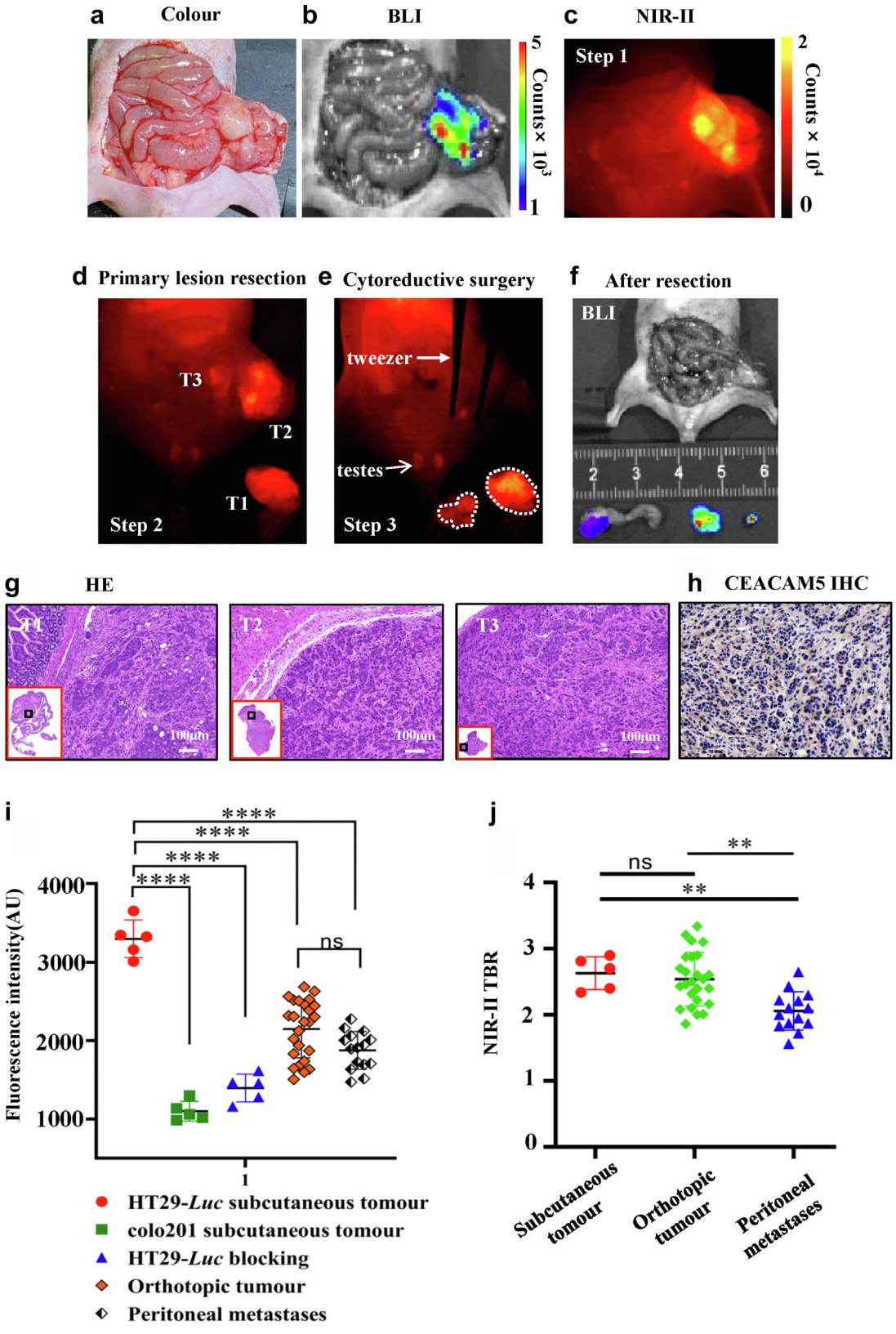
a Colour
b BLI
c NIR-II
Step 1
Counts × 10³
Counts × 10⁴
d Primary lesion resection
e Cytoreductive surgery
f After resection
T3
T2
T1
Step 2
tweezer
testes
Step 3
BLI
g HE
h CEACAM5 IHC
100μm
i
Fluorescence intensity(AU)
****
ns
HT29-Luc subcutaneous tomour
colo201 subcutaneous tomour
HT29-Luc blocking
Orthotopic tumour
Peritoneal metastases
j
NIR-II TBR
ns
**
Subcutaneous tomour
Orthotopic tumour
Peritoneal metastases

positive for CEACAM5 (Fig. 6g and h). We quantified the fluorescence intensity of all orthotopic tumours (n = 25) and peritoneal metastases (n = 15), found no significant difference (2120.30 ± 391.33 *vs.* 1900.33 ± 227.19, P = 0.4193, Student's t-test). However, compared with subcutaneous tumours, the fluorescent signal of orthotopic tumours and peritoneal metastatic tumours was weaker, and there is a significant difference (P < 0.001, Student's t-test, Fig. 6i). Finally, we calculated the TBR of orthotopic tumours, peritoneal metastases, and subcutaneous tumours, and found that the TBR of peritoneal metastases was lower than that of orthotopic tumours (2.06 ± 0.29 *vs.* 2.54 ± 0.41, P < 0.01, Student's t-test, Fig. 6j).

Human colorectal cancer fresh specimens incubated with 2D5-IRDye800CW

We collected 5 cases of colorectal cancer biopsy specimens under endoscopy and 10 cases of fresh colorectal cancer specimens resected during surgery. After incubation with 2D5-IRDye800CW, endoscopic biopsy specimens showed high fluorescence intensity in 4/5 cases and positive immunohistochemical results for CEACAM5 (S1). The probe incubation results of the specimens resected during the operation showed that fluorescence intensity of the tumour tissue in the same patient was significantly higher than that of the adjacent normal intestines (Fig. 7a–f), and there was a statistical difference (Fig. 7g). High fluorescence signal was found in 7 out of 10 tumor tissues, and the immunohistochemical results of CEACAM5 were shown as S2.

Confocal microscopy of human colorectal cancer specimens

It was verified that 2D5-IRDye800CW can specifically bind to CEACAM5-positive human colorectal cancer specimens. We performed frozen sections of the incubated isolated human colorectal cancer specimens to verify the binding of 2D5-IRDye800CW to tumour cells at the microscopic level. Confocal microscopy imaging results showed a strong 2D5-IRDye800CW fluorescence signal (Fig. 8e, red) on tumour tissue, but no fluorescence signal in normal tissue (Fig. 8a–i). Pathological HE staining and CEACAM5 immunohistochemical results showed that CEACAM5 was positive and highly expressed in tumour tissue, and CEACAM5 was negative in normal tissue (Fig. 8j–o).

Discussion

Fluorescence-guided surgery is rapidly entering clinical practice, but most studies have focused on the NIR-I (700–900 nm) window with a limited imaging resolution and depth.[39] Because of reduced scattering, minimal absorption and negligible autofluorescence, NIR-II imaging provides high resolution, a high signal-to-noise ratio, and deep tissue penetration capability.[40,41] The first-in-human clinical study of NIR-II fluorescence-guided liver cancer resection has been achieved, and the results show that NIR-II imaging has greater advantages over conventional NIR-I imaging in clinical scenarios.[42]

In this study, we demonstrated a colorectal cancer-specific NIR-II probe 2D5-IRDye800CW, which was synthesized by conjugating the anti-CEACAM5 nanobody 2D5 and the fluorescent dye IRDye800CW. *In vitro* and *in vivo* studies showed that 2D5-IRDye800CW (i) has excellent NIR-II (1000 nm–1600 nm) imaging capabilities, exhibiting higher resolution and less tissue scattering; *in vivo* tumour imaging had a higher TBR, 2.55 ± 0.38 (NIR-II) *vs.* 1.94 ± 0.20 (NIR-I), P < 0.001, Student's t-test; (ii) binds to CEACAM5-positive colorectal cancer tumour cells with a high affinity (2.29 nM) and high specificity, but does not accumulate in CEACAM5 (–) tumour tissue; (iii) has high penetration and can quickly reach the tumour area within 15 min after intravenous injection (S3) and allows real-time fluorescence image-guided surgery (FGS) on the day after injection (2–24 hours), tumour fluorescence is retained for more than 48 hours, allowing intraoperative, preoperative and postoperative visualization of the tumour and blood vessels throughout the surgical process; (iv) achieves accurate identification and resection of residual tumour lesions and peritoneum metastatic lesions (<2 mm); and (v) can specifically target CEACEAM5-positive human colorectal cancer specimens *in vitro*, and the tumour fluorescence signal intensity is positively correlated with the immunohistochemical results of CEACAM5.

Several colorectal cancer-targeted fluorescent probes have entered clinical trials, such as bevacizumab-IRDye800CW, SGM101 and [111In] In-DOTA-labetuzumab-IRDye800CW,[10,43,44] these targeting probes are bound by large molecular weight monoclonal antibodies which have longer half-lives, resulting in the generation of non-specific background signals, peak fluorescence accumulation at the tumour and an overall delay in the clearance of unbound probes. In order to perform surgery at the optimal imaging time point, targeted probes need to be injected at 2–4 days or even at 4–6 days before surgery; it is not conducive to complete imaging in a short period of time in specific clinical scenarios such as ordinary endoscopy. CEA is considered to be the preferred biomarker for targeting colorectal cancer

Fig. 6: NIR-II fluorescence-guided surgery for colorectal peritoneal cancer. (a–c) Intraoperative white light, BLI and NIR-II imaging. (d, e) Primary tumour resection under NIR-II fluorescence guidance (d, T1), then complete resection of peritoneal metastases and abdominal residual tumour (e, T2, T3). (f) BLI imaging after surgery. (g, h) Pathological results of all resected tumours and immunohistochemical staining for CEACAM5. (i) Fluorescence intensity of all orthotopic tumours (n = 25) and peritoneal metastases (n = 15), subcutaneous tumours (n = 15). (j) TBR of orthotopic tumours, peritoneal metastases, and subcutaneous tumours.

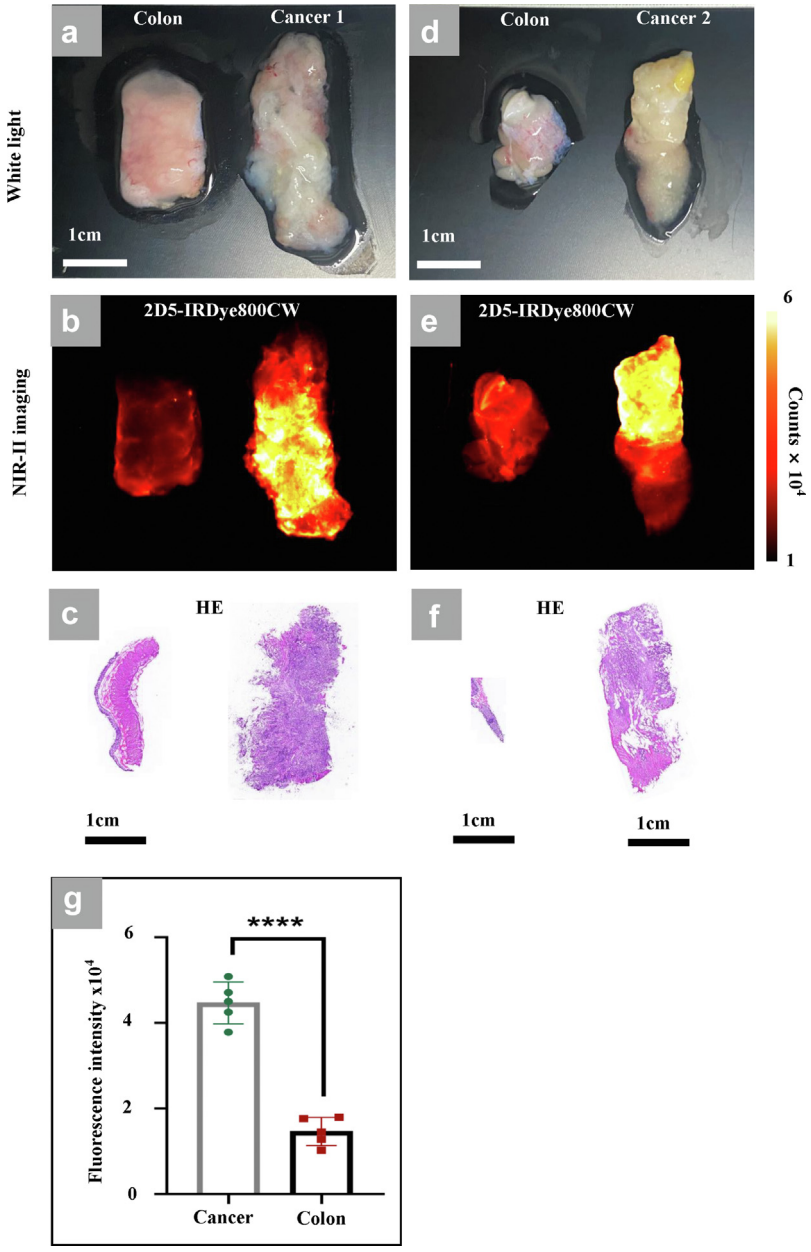

Fig. 7: Human colorectal cancer specimens incubated with 2D5-IRDye800CW. (a, d) White light image of isolated colorectal cancer tissue and adjacent normal colorectal tissue. (b, e) NIR-II image after incubation with 2D5-IRDye800CW. (c) Pathological HE staining results (a). (f) Pathological HE staining results (d). (g) Fluorescence intensity of the tumour and adjacent intestinal tissue. Statistical analysis (Student's t-test) with $P < 0.05$ (*) was regarded as statistically significant.

in vivo, so we chose anti-CEACAM5 nanobody with a small molecular weight to construct imaging probes, which have the characteristics of high stability, high affinity, rapid metabolism and high permeability.[45–47] It is conducive to rapid imaging to achieve imaging results on the same day of administration. 2D5-IRDye800CW can be rapidly combined with CEACAM5 overexpressing tumour cells after 15–30 min injection into the tail vein, which the fluorescence signal (TBR = 1.7) of subcutaneous tumours is higher than that of the surrounding skin, showing the ability of high permeability and rapid imaging ability. More importantly, the tumour tissue still has a certain intensity of the fluorescent signal (TBR = 2.1) 48 hours after injection, and the 2–48 hours imaging window provides flexibility in the scheduling and execution of probe injections and

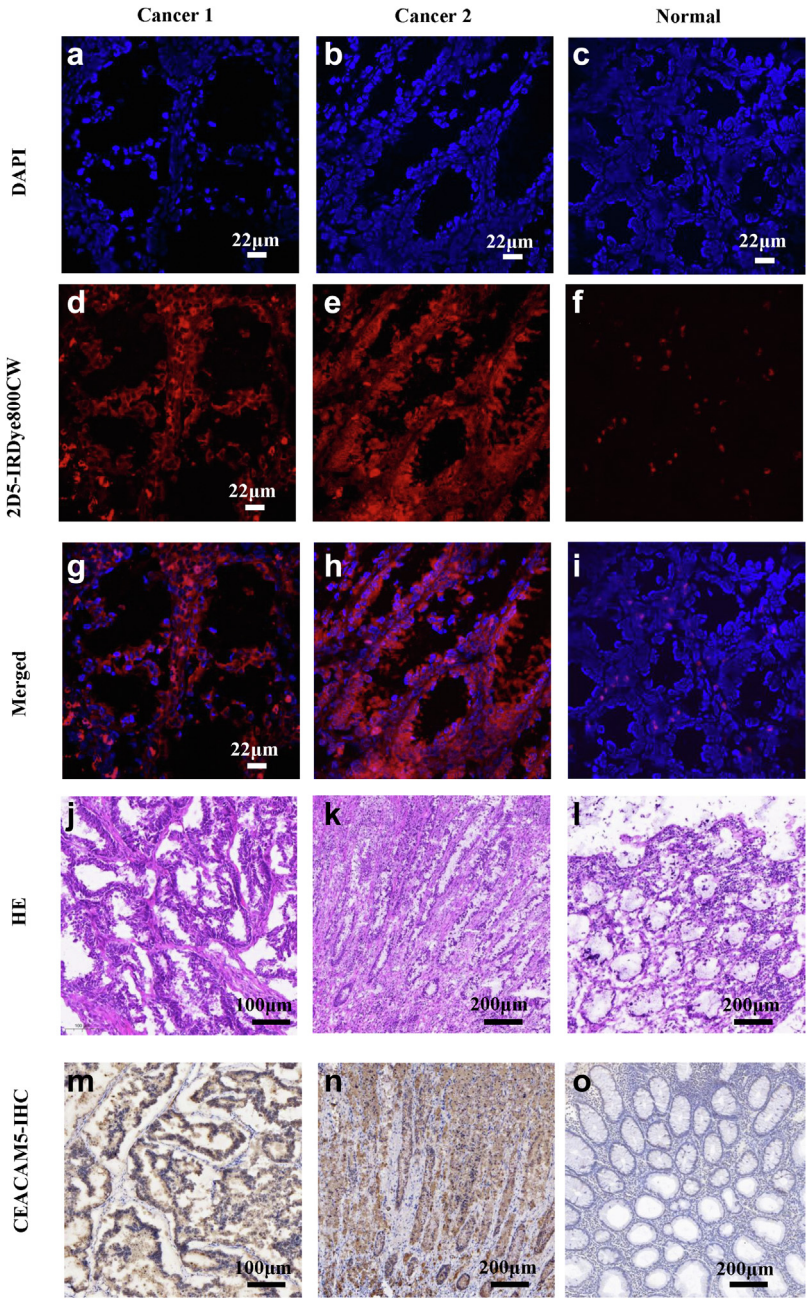

Fig. 8: Microscopic imaging of human colorectal cancer tissue incubated with 2D5-IRDye800CW. (a–c) DAPI staining of human colorectal cancer and normal tissue nucleus (blue). (d–f) Confocal imaging results of 2D5-IRDye800CW incubated with the specimen. (g–i) Colorectal cancer and normal tissue nuclear staining merged with the probe pseudocolor image. (j–l) Pathological HE staining of colorectal cancer and normal tissue. (m–o) Immunohistochemical staining of CEACAM5 in colorectal cancer and normal tissue.

surgical procedures. In addition, its ability to rapidly image and its small molecular weight enable topical delivery, which is the easiest way to administer FGS-targeted drugs.

Due to the probe quickly accumulated in the kidneys after being injected into mice, the fluorescence intensity of the kidneys is much higher than the tumour region in the early stage of imaging, resulting in the masking of the tumour signal adjacent to the spatial location of the kidneys. However, when the colorectal orthotopic model is used for imaging, the anatomical position of the kidneys is relatively deep, and it is difficult for the

fluorescence signal of the kidneys to penetrate the intestinal tissue covering the kidneys. Therefore, the kidneys can be hidden to reduce the influence of the tumour tissue signal.[48]

Although NIR-II fluorophores exhibit excellent imaging capabilities, however, existing NIR-II fluorophores, including semiconducting inorganic nanomaterials and recently introduced small-molecule organic dyes face significant technical and regulatory hurdles before clinical translation.[49,50] Recent studies on the spectral characterization of NIR-I dyes such as indocyanine green (ICG), IRDye800CW, and IR-12N3 have revealed long emission tails extending beyond the 1500 nm NIR-II region, which opens up a whole new avenue for clinical NIR-II imaging.[22,37,51] Our study demonstrates the imaging capability of the 2D5-IRDye800CW at 1000 nm–1500 nm with deeper tissue penetration and higher spatial resolution, which is beneficial for intraoperative imaging of deeper tissue and fine blood vessels. However, we should also note that the imaging time of 2D5-IRDye800CW in NIR-II sacrifices a certain imaging time, the exposure time at 1000 nm is 30 ms, and the exposure time is 2 s when imaging at 1500 nm.

There are still some limitations of this study when comparing the difference between white light and NIR-II-guided tumour resection; there is a lack of comparison of data such as recurrence rate in subsequent survival. In addition, all mouse orthotopic models adopt the imaging method of the open abdominal cavity, while clinical laparoscopy has been widely used in colorectal cancer surgery. This is because the equipment that is currently available for NIR-II intraoperative navigation is open abdominal visual field imaging. This study explored the application value of the NIR-II imaging modality in CRC. Fluorescence endoscopy for intraoperative navigation of NIR-II has been developed and will accelerate the clinical translation of NIR-II.[52]

Contributors

Study design: Tian Jie, Zhenhua Hu, Haifeng Liu, Jianqiang Tang.

Literature search: Xiaoyong Guo, Xiaohua Jia, Miaomiao Li, Zeyu Zhang.

Data collection: Xiaoyong Guo, Changjian Li, Xiaohua Jia, Yawei Qu, Qiaojun Qu, Shuangling Luo.

Data analysis: all authors.

Data interpretation: all authors.

Figures: Xiaoyong Guo, Changjian Li, Xiaohua Jia, Yawei Qu, Caiguang Cao.

Writing: Xiaoyong Guo, Changjian Li, Xiaohua Jia, Yawei Qu.

Revise: Xiaoyong Guo, Xiaohua Jia, Changjian Li, Jianqiang Tang.

Access and verification of the data: all authors.

Responsibilities for the decision to submit the manuscript: all authors.

All authors reviewed, discussed, and agreed with manuscript.

Data sharing statement

The main data supporting the results of this study are available within the paper and its Supplementary materials. The raw near-infrared fluorescence images can be obtained after asking the corresponding authors and clarifying the purpose of use.

Declaration of interests

The authors declare that they have no conflicts of interest.

Acknowledgments

This study was supported by Beijing Natural Science Foundation (JQ19027), the National Key Research and Development Program of China (2017YFA0205200), National Natural Science Foundation of China (NSFC) (61971442, 62027901, 81930053, 92059207, 81227901, 82102236), Beijing Natural Science Foundation (L222054), CAS Youth Interdisciplinary Team (JCTD-2021-08), the Strategic Priority Research Program of the Chinese Academy of Sciences (XDA16021200), the Zhuhai High-level Health Personnel Team Project (Zhuhai HLHPTP201703), the Fundamental Research Funds for the Central Universities (JKF-YG-22-B005) and Capital Clinical Characteristic Application Research (Z181100001718178). The authors would like to acknowledge the instrumental and technical support of the multi-modal biomedical imaging experimental platform, Institute of Automation, Chinese Academy of Sciences.

We would like to thank Professor Zhen Cheng from the Center for Molecular Imaging, Shanghai Institute of Materia Medica, Chinese Academy of Sciences, for his help with probe synthesis and characterization.

Appendix A. Supplementary data

Supplementary data related to this article can be found at https://doi.org/10.1016/j.ebiom.2023.104476.

References

1 Sung H, Ferlay J, Siegel RL, et al. Global cancer statistics 2020: GLOBOCAN estimates of incidence and mortality worldwide for 36 cancers in 185 countries. *CA Cancer J Clin*. 2021;71(3):209–249.
2 Siegel RL, Miller KD, Fuchs HE, Jemal A. Cancer statistics, 2022. *CA Cancer J Clin*. 2022;72(1):7–33.
3 Amri R, Bordeianou LG, Sylla P, Berger DL. Association of radial margin positivity with colon cancer. *JAMA Surg*. 2015;150(9):890–898.
4 Orosco RK, Tapia VJ, Califano JA, et al. Positive surgical margins in the 10 most common solid cancers. *Sci Rep*. 2018;8(1):5686.
5 Galema HA, Meijer RPJ, Lauwerends LJ, et al. Fluorescence-guided surgery in colorectal cancer; a review on clinical results and future perspectives. *Eur J Surg Oncol*. 2021;48:810.
6 Blair S, Garcia M, Davis T, et al. Hexachromatic bioinspired camera for image-guided cancer surgery. *Sci Transl Med*. 2021;13(592):eaaw7076.
7 Segelman J, Granath F, Holm T, Machado M, Mahteme H, Martling A. Incidence, prevalence and risk factors for peritoneal carcinomatosis from colorectal cancer. *Br J Surg*. 2012;99(5):699–705.
8 Quénet F, Elias D, Roca L, et al. Cytoreductive surgery plus hyperthermic intraperitoneal chemotherapy versus cytoreductive surgery alone for colorectal peritoneal metastases (PRODIGE 7): a multicentre, randomised, open-label, phase 3 trial. *Lancet Oncol*. 2021;22(2):256–266.
9 de Valk KS, Deken MM, Handgraaf HJM, et al. First-in-human assessment of cRGD-ZW800-1, a zwitterionic, integrin-targeted, near-infrared fluorescent peptide in colon carcinoma. *Clin Cancer Res*. 2020;26(15):3990–3998.
10 Boogerd LSF, Hoogstins CES, Schaap DP, et al. Safety and effectiveness of SGM-101, a fluorescent antibody targeting carcinoembryonic antigen, for intraoperative detection of colorectal cancer: a dose-escalation pilot study. *Lancet Gastroenterol Hepatol*. 2018;3(3):181–191.
11 Mieog JSD, Achterberg FB, Zlitni A, et al. Fundamentals and developments in fluorescence-guided cancer surgery. *Nat Rev Clin Oncol*. 2022;19(1):9–22.
12 Lauwerends LJ, van Driel PBAA, Baatenburg de Jong RJ, et al. Real-time fluorescence imaging in intraoperative decision making for cancer surgery. *Lancet Oncol*. 2021;22(5):e186–e195.
13 Li C, Mi J, Wang Y, et al. New and effective EGFR-targeted fluorescence imaging technology for intraoperative rapid determination of lung cancer in freshly isolated tissue. *Eur J Nucl Med Mol Imaging*. 2022;50:494.
14 van Dam GM, Themelis G, Crane LM, et al. Intraoperative tumor-specific fluorescence imaging in ovarian cancer by folate

receptor-alpha targeting: first in-human results. *Nat Med*. 2011;17(10):1315–1319.
15 de Jongh SJ, Tjalma JJJ, Koller M, et al. Back-table fluorescence-guided imaging for circumferential resection margin evaluation using bevacizumab-800CW in patients with locally advanced rectal cancer. *J Nucl Med*. 2020;61(5):655–661.
16 Lu G, van den Berg NS, Martin BA, et al. Tumour-specific fluorescence-guided surgery for pancreatic cancer using panitumumab-IRDye800CW: a phase 1 single-centre, open-label, single-arm, dose-escalation study. *Lancet Gastroenterol Hepatol*. 2020;5(8):753–764.
17 Schaap DP, de Valk KS, Deken MM, et al. Carcinoembryonic antigen-specific, fluorescent image-guided cytoreductive surgery with hyperthermic intraperitoneal chemotherapy for metastatic colorectal cancer. *Br J Surg*. 2020;107(4):334–337.
18 He K, Hong X, Chi C, et al. Efficacy of near-infrared fluorescence-guided hepatectomy for the detection of colorectal liver metastases: a randomized controlled trial. *J Am Coll Surg*. 2022;234(2):130–137.
19 He K, Li P, Zhang Z, et al. Intraoperative near-infrared fluorescence imaging can identify pelvic nerves in patients with cervical cancer in real time during radical hysterectomy. *Eur J Nucl Med Mol Imaging*. 2022;49(8):2929–2937.
20 Yang RQ, Lou KL, Wang PY, et al. Surgical navigation for malignancies guided by near-infrared-II fluorescence imaging. *Small Methods*. 2021;5(3):e2001066.
21 Antaris AL, Chen H, Cheng K, et al. A small-molecule dye for NIR-II imaging. *Nat Mater*. 2016;15(2):235–242.
22 Zhu S, Hu Z, Tian R, et al. Repurposing cyanine NIR-I dyes accelerates clinical translation of near-infrared-II (NIR-II) bioimaging. *Adv Mater*. 2018:e1802546.
23 Cao C, Jin Z, Shi X, et al. First clinical investigation of near-infrared window IIa/IIb fluorescence imaging for precise surgical resection of gliomas. *IEEE Trans Biomed Eng*. 2022;69(8):2404–2413.
24 Yang J, He S, Hu Z, et al. In vivo multifunctional fluorescence imaging using liposome-coated lanthanide nanoparticles in near-infrared-II/IIa/IIb windows. *Nano Today*. 2021;38.
25 Shi X, Zhang Z, Zhang Z, et al. Near-infrared window II fluorescence image-guided surgery of high-grade gliomas prolongs the progression-free survival of patients. *IEEE Trans Biomed Eng*. 2022;69(6):1889–1900.
26 Qu Q, Zhang Z, Guo X, et al. Novel multifunctional NIR-II aggregation-induced emission nanoparticles-assisted intraoperative identification and elimination of residual tumor. *J Nanobiotechnology*. 2022;20(1):143.
27 Cao C, Deng S, Wang B, et al. Intraoperative near-infrared II window fluorescence imaging-assisted nephron-sparing surgery for complete resection of cystic renal masses. *Clin Transl Med*. 2021;11(10):e604.
28 Chang B, Li D, Ren Y, et al. A phosphorescent probe for in vivo imaging in the second near-infrared window. *Nat Biomed Eng*. 2022;6(5):629–639.
29 Ji A, Lou H, Qu C, et al. Acceptor engineering for NIR-II dyes with high photochemical and biomedical performance. *Nat Commun*. 2022;13(1):3815.
30 de Valk KS, Deken MM, Schaap DP, et al. Dose-finding study of a CEA-targeting agent, SGM-101, for intraoperative fluorescence imaging of colorectal cancer. *Ann Surg Oncol*. 2021;28(3):1832–1844.
31 Tiernan JP, Perry SL, Verghese ET, et al. Carcinoembryonic antigen is the preferred biomarker for in vivo colorectal cancer targeting. *Br J Cancer*. 2013;108(3):662–667.
32 Li B, Zhao M, Lin J, Huang P, Chen X. Management of fluorescent organic/inorganic nanohybrids for biomedical applications in the NIR-II region. *Chem Soc Rev*. 2022;51(18):7692–7714.
33 Yang Y, Zhang F. Molecular fluorophores for in vivo bioimaging in the second near-infrared window. *Eur J Nucl Med Mol Imaging*. 2022;49(9):3226–3246.
34 Lin J, Yu J, Wang H, et al. Development of a highly thermostable immunoassay based on a nanobody-alkaline phosphatase fusion protein for carcinoembryonic antigen detection. *Anal Bioanal Chem*. 2020;412(8):1723–1728.
35 Zhao J, Sjölander A, Edgren G. Mortality among patients undergoing blood transfusion in relation to donor sex and parity: a natural experiment. *JAMA Intern Med*. 2022;182(7):747–756.
36 Gutowski M, Framery B, Boonstra MC, et al. SGM-101: an innovative near-infrared dye-antibody conjugate that targets CEA for fluorescence-guided surgery. *Surg Oncol*. 2017;26(2):153–162.
37 Carr JA, Franke D, Caram JR, et al. Shortwave infrared fluorescence imaging with the clinically approved near-infrared dye indocyanine green. *Proc Natl Acad Sci U S A*. 2018;115(17):4465–4470.
38 Di Nicolantonio F, Vitiello PP, Marsoni S, et al. Precision oncology in metastatic colorectal cancer–from biology to medicine. *Nat Rev Clin Oncol*. 2021;18(8):506–525.
39 Hernot S, van Manen L, Debie P, Mieog JSD, Vahrmeijer AL. Latest developments in molecular tracers for fluorescence image-guided cancer surgery. *Lancet Oncol*. 2019;20:e354.
40 He S, Song J, Qu J, Cheng Z. Crucial breakthrough of second near-infrared biological window fluorophores: design and synthesis toward multimodal imaging and theranostics. *Chem Soc Rev*. 2018;47(12):4258–4278.
41 Hu Z, Chen WH, Tian J, Cheng Z. NIRF nanoprobes for cancer molecular imaging: approaching clinic. *Trends Mol Med*. 2020;26(5):469–482.
42 Hu Z, Fang C, Li B, et al. First-in-human liver-tumour surgery guided by multispectral fluorescence imaging in the visible and near-infrared-I/II windows. *Nat Biomed Eng*. 2020;4(3):259–271.
43 de Gooyer JM, Elekonawo FMK, Bremers AJA, et al. Multimodal CEA-targeted fluorescence and radioguided cytoreductive surgery for peritoneal metastases of colorectal origin. *Nat Commun*. 2022;13(1):2621.
44 Lamberts LE, Koch M, de Jong JS, et al. Tumor-specific uptake of fluorescent bevacizumab-IRDye800CW microdosing in patients with primary breast cancer: a phase I feasibility study. *Clin Cancer Res*. 2017;23(11):2730–2741.
45 Debie P, Lafont C, Defrise M, et al. Size and affinity kinetics of nanobodies influence targeting and penetration of solid tumours. *J Control Release*. 2020;317:34–42.
46 Barakat S, Berksoz M, Zahedimaram P, Piepoli S, Erman B. Nanobodies as molecular imaging probes. *Free Radic Biol Med*. 2022;182:260–275.
47 Erreni M, Schorn T, D'Autilia F, Doni A. Nanobodies as versatile tool for multiscale imaging modalities. *Biomolecules*. 2020;10(12):1695.
48 Lwin TM, Hernot S, Hollandsworth H, et al. Tumor-specific near-infrared nanobody probe rapidly labels tumors in an orthotopic mouse model of pancreatic cancer. *Surgery*. 2020;168(1):85–91.
49 Li C, Guan X, Zhang X, et al. NIR-II bioimaging of small molecule fluorophores: from basic research to clinical applications. *Biosens Bioelectron*. 2022;216:114620.
50 Liu Y, Li Y, Koo S, et al. Versatile types of inorganic/organic NIR-IIa/IIb fluorophores: from strategic design toward molecular imaging and theranostics. *Chem Rev*. 2022;122(1):209–268.
51 Zhu S, Yung BC, Chandra S, Niu G, Antaris AL, Chen X. Near-infrared-II (NIR-II) bioimaging via off-peak NIR-I fluorescence emission. *Theranostics*. 2018;8(15):4141–4151.
52 Suo Y, Wu F, Xu P, et al. NIR-II Fluorescence Endoscopy for Targeted Imaging of Colorectal Cancer. *Adv Healthc Mater*. 2019;8(23):e1900974.